Supplementary Table 1. Known Clinically Relevant Genomic Alterations. HDEL=Copy Number less than 1; HAMP=Copy Number greater than 4

Model	Clinical Relevant Alterations
BCX.010	PI3KCA H1047R, PTEN HDEL
BCX.011	FGFR1 HAMP, PTEN N276S, ATM HDEL
BCX.017	PIK3CA HAMP, CCNE1 HAMP, PIK3R1 HDEL
BCX.022	ATM HDEL, BRCA2 HDEL, CDKN2A, FGFR1 HAMP, NOTCH2 HAMP, PIK3R1 HDEL
BCX.024	PTEN HDEL
BCX.070	CCNE1 HAMP, AKT2 HAMP, NOTCH1 K2156*, ATM DEL, BRCA2 HDEL, STK11 HDEL
BCX.087	None
BCX.094	STK11 HDEL, BRCA2 HDEL

Supplementary Table 2. Genes differentially expressed at baseline by RNAseq between PDXs more sensitive and less sensitive to OXPHOS. Positive numbers indicate higher expression in less sensitive models.

	log2FoldChange	padj
TWIST1	8.22	1.33E-05
LMX1B	-6.03	2.54E-05
SEMA5A	7.58	4.61E-05
ZFPM2	6.67	4.61E-05
NAV3	6.83	4.85E-05
PVRL4	-4.53	6.51E-05
THY1	7.58	7.05E-05
LY96	6.82	8.02E-05
CXCL16	-4.25	8.02E-05
ASXL3	7.40	8.88E-05
ST8SIA4	6.53	0.00012
ADAMTS6	5.99	0.00012
CLGN	5.14	0.00014
PLXDC1	6.42	0.00014
AXL	6.32	0.00014
ZMYND15	-5.97	0.00014
TENM4	6.59	0.000144
PCDH7	6.13	0.000147
PIK3C2B	-3.27	0.000181
RP11-366L20.2	7.16	0.000222
RAB31	5.14	0.000222
KCNE4	6.80	0.000222
SERPINI1	4.36	0.000312
KLK6	-6.81	0.000312
MPZL3	-3.43	0.000316
HSD17B11	6.20	0.000316
HOXD8	7.12	0.000319
KIAA1009	2.16	0.000339
CDH2	5.94	0.000339
GPR176	4.81	0.000375
NPFFR2	6.94	0.000396
SLC44A2	-2.72	0.000396
IGF2BP1	6.81	0.000531
PRSS35	6.28	0.000539
AC003986.6	6.84	0.000613
RP11-553A21.3	4.46	0.000769

TGFB1	4.60	0.000815
LAD1	-4.73	0.000874
RP11-152P17.2	6.25	0.000874
TNFRSF18	-4.98	0.000886
MMP1	6.94	0.000886
TJP3	-4.67	0.000886
LPHN3	5.68	0.000958
GNG11	6.29	0.001085
SPOCK3	6.78	0.001112
IGFBP6	6.03	0.001112
AKAP12	5.43	0.001186
LRRC17	5.43	0.001186
CACNA2D1	5.64	0.001234
CLDN10	5.97	0.001396
DIO2	-5.22	0.001493
SLC2A3	5.49	0.001493
CCDC102B	4.70	0.001493
RP11-227D13.1	5.75	0.001493
CCBE1	5.91	0.00153
SOCS2	4.65	0.001784
CHN2	5.30	0.001838
RP11-544M22.8	-4.01	0.001899
RUNX2	5.20	0.001945
SEMA3A	5.94	0.001978
RFX8	6.48	0.001989
GUCY1A2	5.67	0.002009
KIAA1522	-2.42	0.002237
STON2	4.12	0.002237
CCDC85C	-2.32	0.002237
KRTAP5-AS1	-4.20	0.002237
ABLIM2	-4.36	0.002237
LINC00941	5.51	0.002237
MEDAG	6.43	0.002237
RP11-600K15.1	6.47	0.002237
TNFAIP8L3	4.48	0.002237
CTD-2008P7.9	-5.77	0.002237
ZEB2	5.72	0.002237

KB-1562D12.1	-5.54	0.002237
EDIL3	5.92	0.002237
TSTD1	-3.26	0.002237
PROCR	4.66	0.002237
COL21A1	5.94	0.002388
PTENP1	5.15	0.002388
NCCRP1	-5.48	0.002424
ILDR1	-4.27	0.002501
DNM3OS	5.94	0.00258
VEGFC	5.07	0.00258
MEFV	5.88	0.002687
LINC01116	6.45	0.002806
SYT1	5.03	0.002806
RAET1L	-4.97	0.002806
CPED1	5.68	0.002806
POU2F3	-4.39	0.002838
BAI3	6.31	0.002852
DMKN	-5.09	0.002852
CNRIP1	5.57	0.002853
LARGE	-3.69	0.002979
HHIP	4.90	0.002984
RGCC	4.36	0.003009
GPRIN2	-4.72	0.003012
PLAG1	5.02	0.003096
R3HCC1L	1.21	0.003136
RGS4	5.69	0.0034
AP000476.1	6.01	0.0034
MIR1255B1	5.52	0.0034
AC156455.1	4.54	0.0034
A2ML1	-5.48	0.0034
CFH	5.89	0.00344
HTR7	5.62	0.003503
ST3GAL2	2.54	0.003536
TRPA1	5.37	0.003709
CLDN4	-3.66	0.003709
TMEM79	-2.59	0.003787
RP11-81H3.2	6.26	0.003919
COL22A1	-6.00	0.004246
PPP1R3G	4.58	0.004257
AP001626.1	-5.92	0.004293
NAP1L3	4.40	0.004293

HTR2A	5.90	0.004293
TMEFF2	5.93	0.004321
GNG12-AS1	3.36	0.004335
BEAN1	5.62	0.004449
RBM47	-3.39	0.004449
LPAR4	6.04	0.004449
HNRNPA1P33	-5.54	0.004449
HLA-DOA	5.24	0.004604
PAX6	3.53	0.004614
GPM6A	5.33	0.004614
PCDH9	4.45	0.004641
SOWAHB	-4.35	0.0048
PDGFRB	5.49	0.0048
LINC00702	5.82	0.004847
SEPT10	1.57	0.004853
PRR15L	-4.16	0.004853
SLC8A1	5.17	0.005012
EPHA5	5.97	0.005044
LARGE-AS1	-4.17	0.005656
RGS13	5.38	0.005666
COL3A1	5.65	0.005666
ITGA1	4.77	0.005666
PGBD5	-4.79	0.005666
PPP1R26	-2.55	0.005666
SLC16A5	4.35	0.005836
B3GALTL	1.93	0.005958
DCN	5.73	0.005958
H2AFY2	-3.06	0.005958
EPHA3	5.92	0.005958
C1QTNF7	4.91	0.005958
OSR2	4.04	0.005958
BMP4	5.60	0.005997
RASAL1	-3.49	0.006015
PARP8	4.61	0.006029
ROBO4	5.65	0.00603
SLC38A4	3.82	0.006034
ABCC9	4.99	0.006046
TRHDE	5.71	0.006101
CCDC64	-3.24	0.006101
RP11-397A16.2	5.86	0.006101
SLC37A1	-2.25	0.006101

PURG	5.54	0.006101
CD9	-2.88	0.006112
RP11-230G5.2	5.80	0.006296

Supplementary Table 3. Pathways correlated with differentially expressed genes between more and less IACS-10759 sensitive models.

Ingenuity Canonical Pathways	-log(p-value)	Overlap
Hepatic Fibrosis / Hepatic Stellate Cell Activation	4.9	8%
Granulocyte Adhesion and Diapedesis	4.41	7%
Bladder Cancer Signaling	4.36	10%
Leukocyte Extravasation Signaling	4.24	7%
Inhibition of Matrix Metalloproteases	4.04	15%
Agranulocyte Adhesion and Diapedesis	3.52	6%
Regulation of the Epithelial-Mesenchymal Transition Pathway	3.52	6%
Sertoli Cell-Sertoli Cell Junction Signaling	3.17	6%
Ephrin A Signaling	3	10%
HIF1α Signaling	2.77	7%
Axonal Guidance Signaling	2.55	4%
Ephrin Receptor Signaling	2.18	5%
Colorectal Cancer Metastasis Signaling	2.07	4%

Supplementary Table 4. Genes differentially expressed in three sensitive models as determined by Nanostring. Shown as Log2 Fold Change IACS-10759 treated to untreated. Positive numbers indicate an increase with treatment; all the overlapping genes increased with treatment.

	BCX.022	BCX.017	BCX.087
ASNS	0.80	1.65	1.45
DDIT3	1.10	2.49	2.61
TRIB3	0.89	1.37	0.93
TUBE1	1.24	1.30	0.68
S100P	1.43	2.49	1.05
C6orf48	1.84	0.76	0.55
ATF3	1.64	0.68	1.42
ZNF277	0.89	0.64	0.65
NFIL3	0.87	0.60	0.78
CCNB1IP1	1.37	0.64	0.95

Supplementary Figure 1

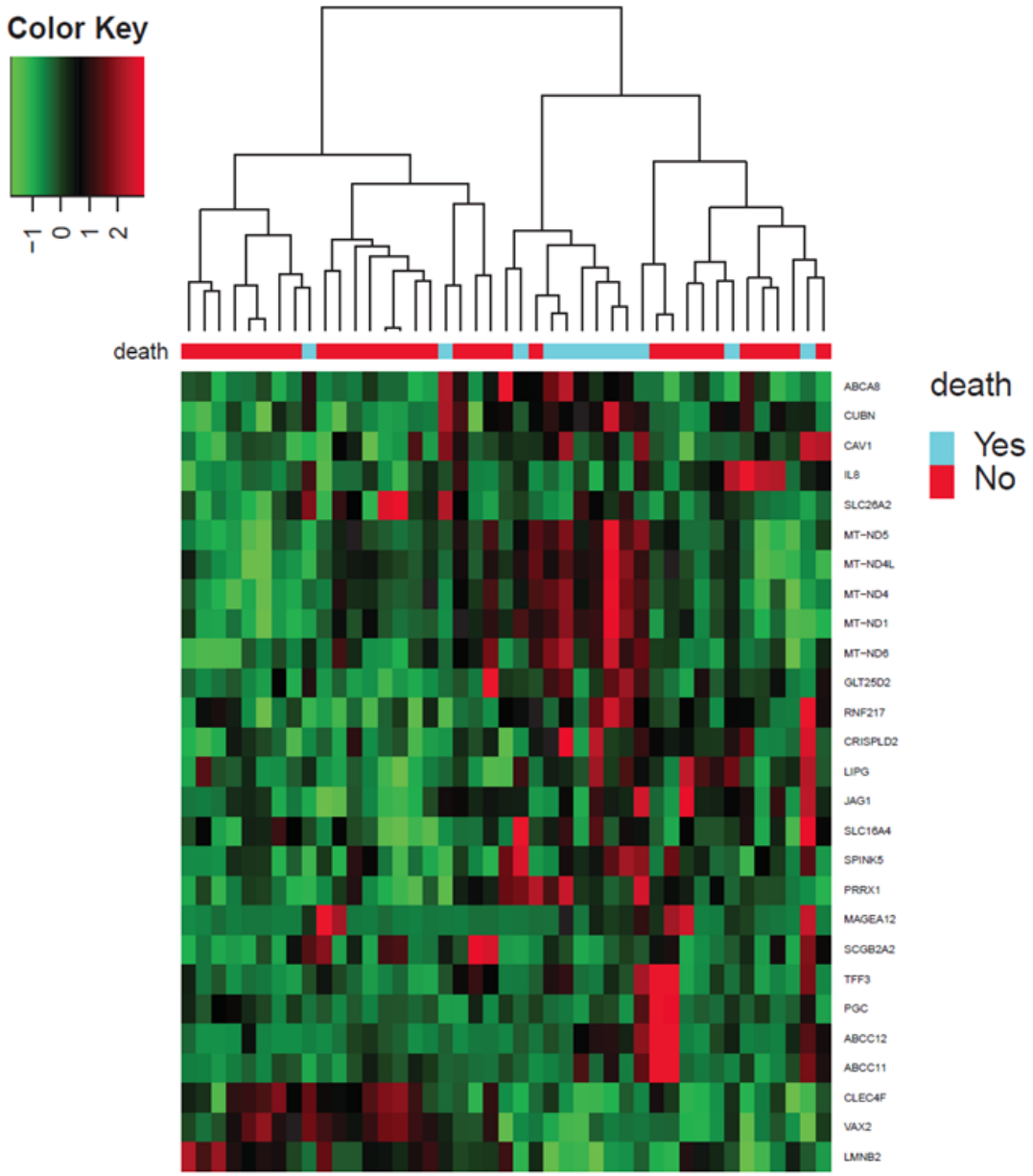

Supplementary Figure 2

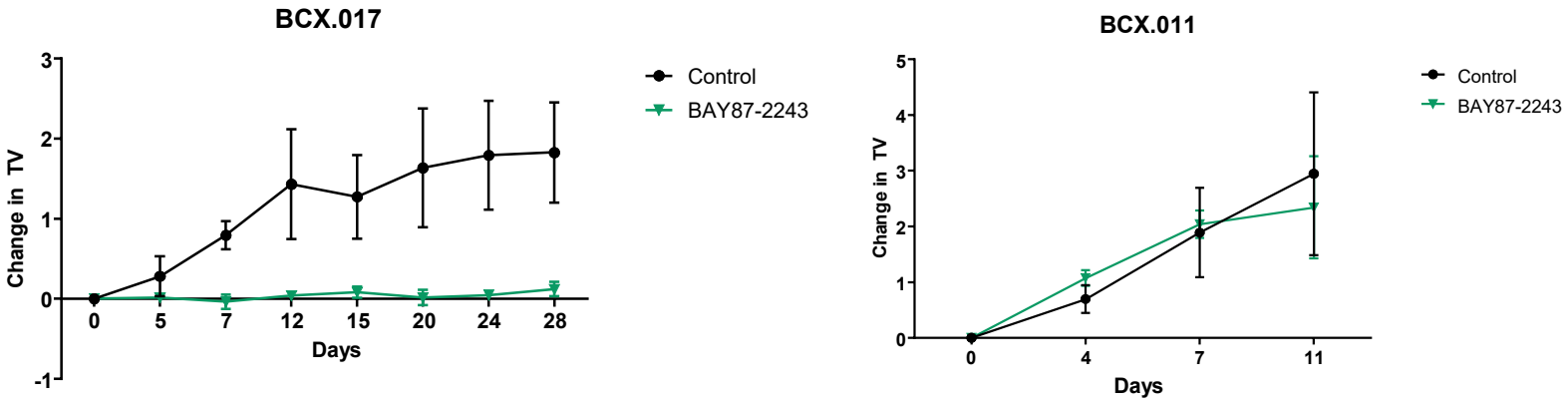

Supplementary Figure 3

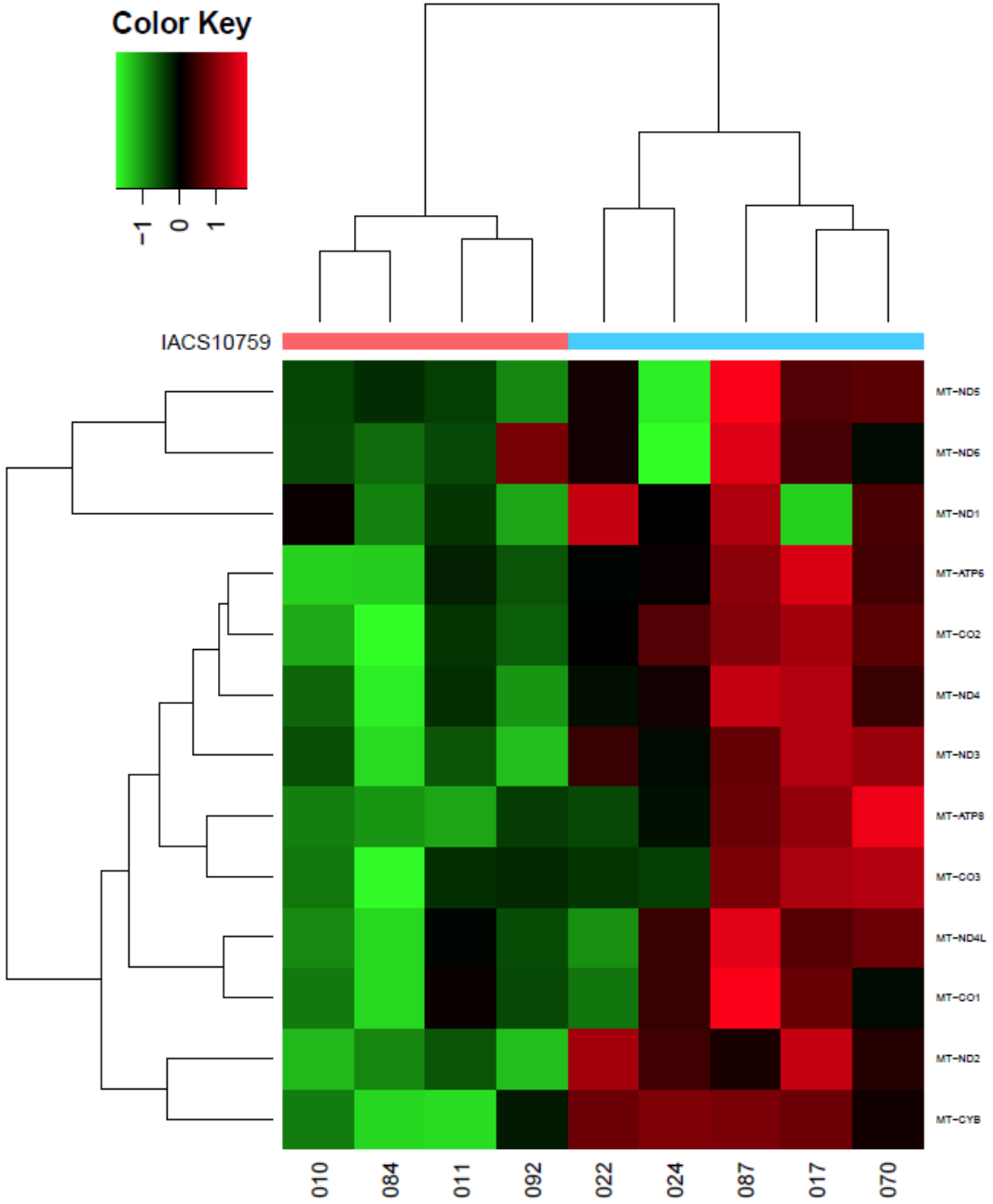

Supplementary Figure 4

A

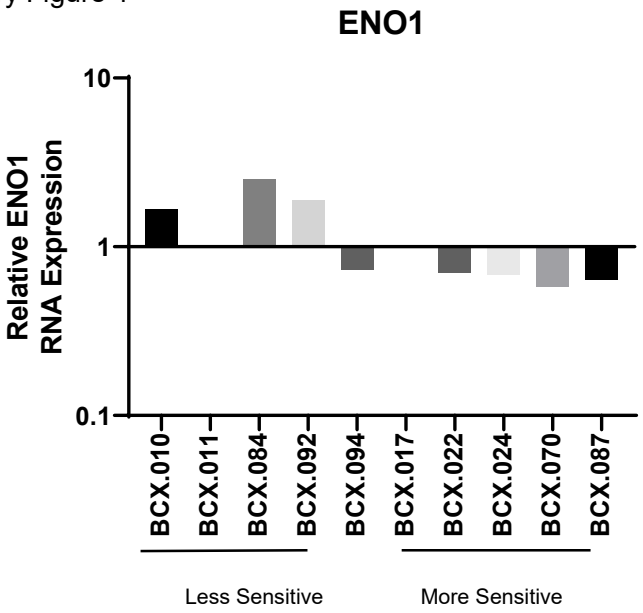

B

		Punch #1		Punch #2		Punch #3	
		Intensity	Extent	Intensity	Extent	Intensity	Extent
More Sensitive	BCX.017	2	100	2	100		
	BCX.022	2	100	2	100	2	100
	BCX.024	2.5	100	2.5	100	2.5	100
	BCX.070	2	100	2	100	2	100
	BCX.087	2	100	2	100	2	100
Less Sensitive	BCX.092	3	100			3	100
	BCX.094	3	100	3	100	3	100
	BCX.084	3	100	3	100	3	100
	BCX.010	3	100	3	100	3	100
	BCX.011	3	100	3	100	3	100

Supplementary Figure 5

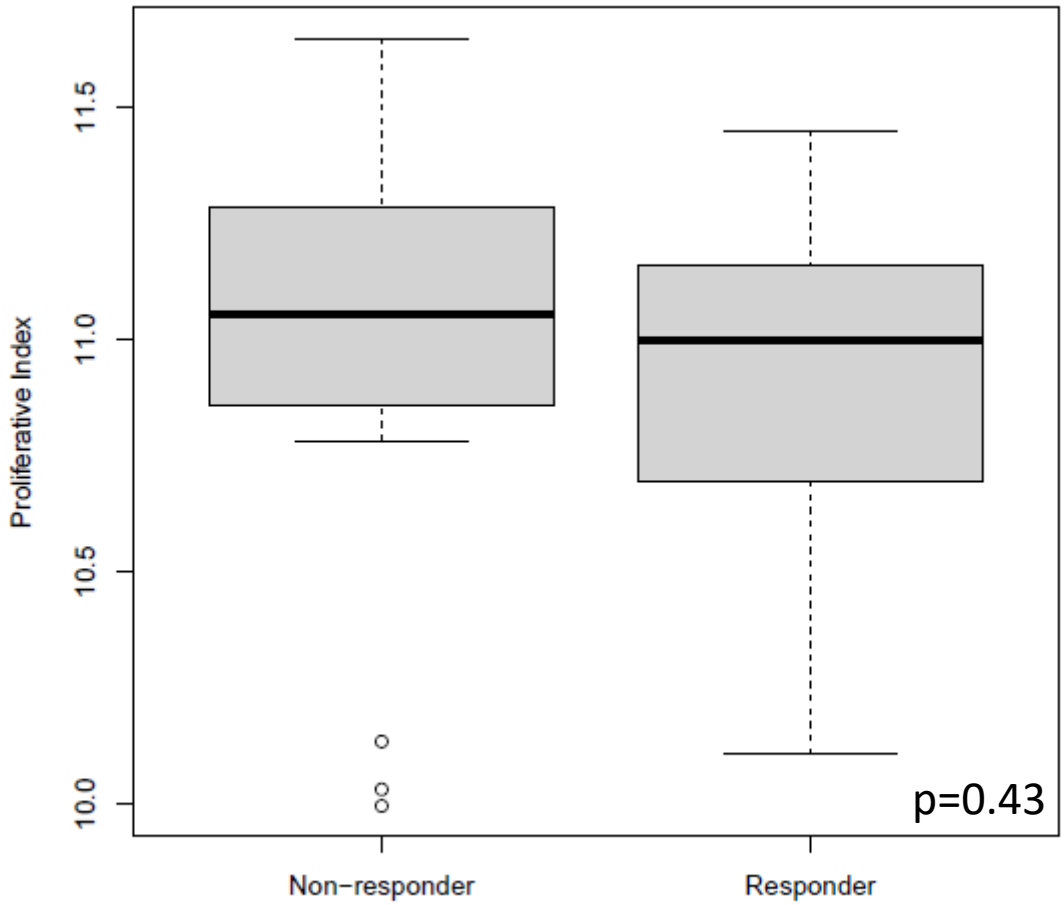

Supplementary Figure 6

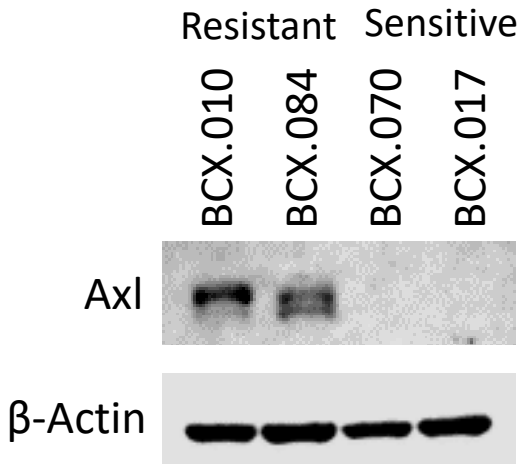

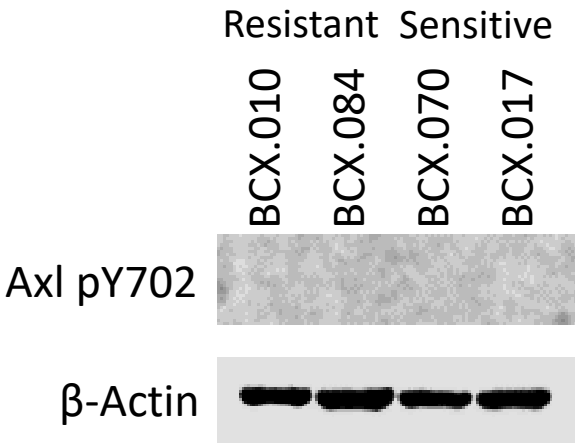

Supplementary Figure 7

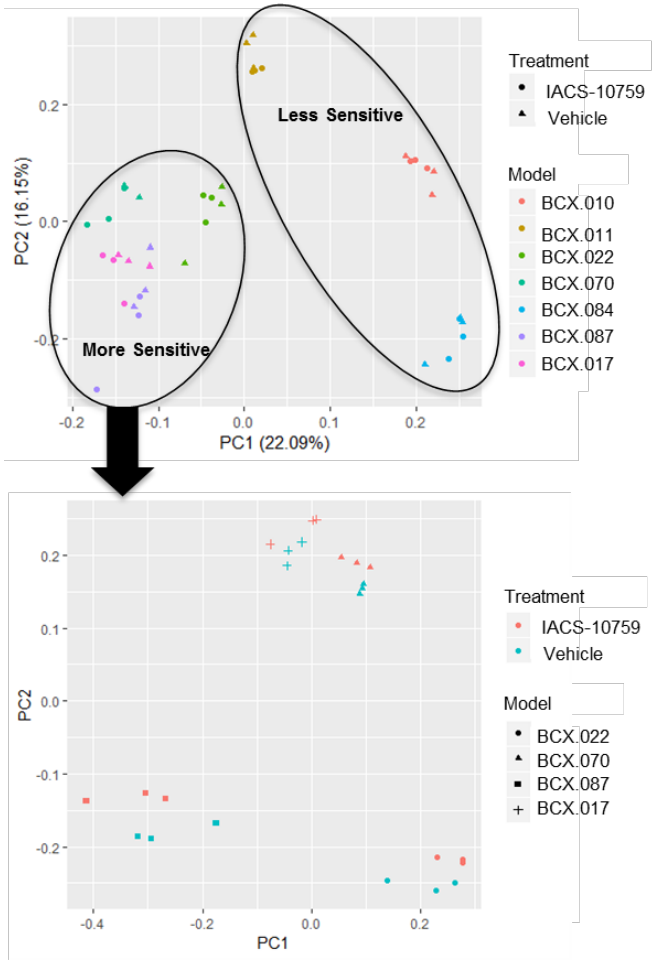

Supplementary Figure 8

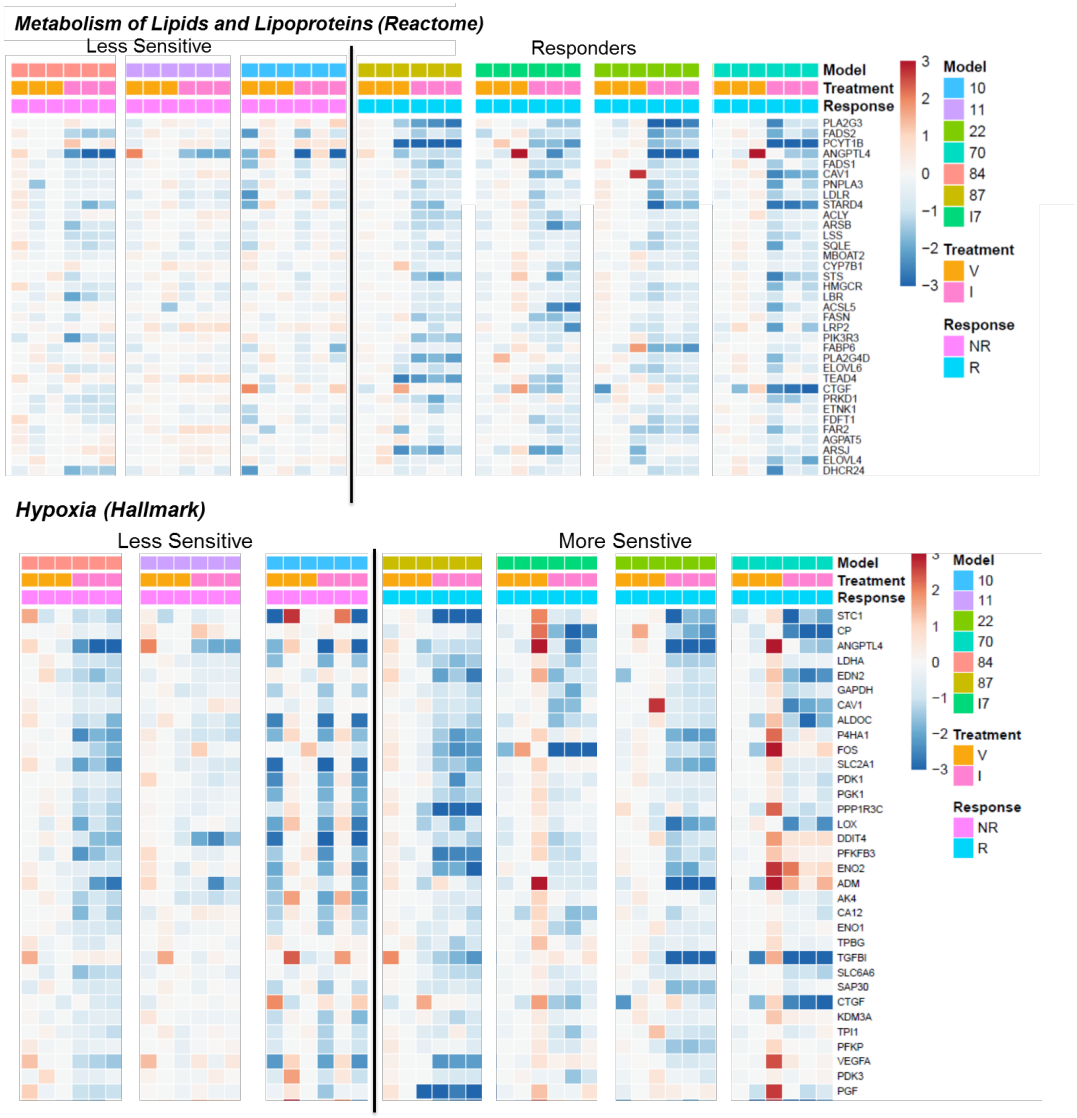

Supplementary Figure 9

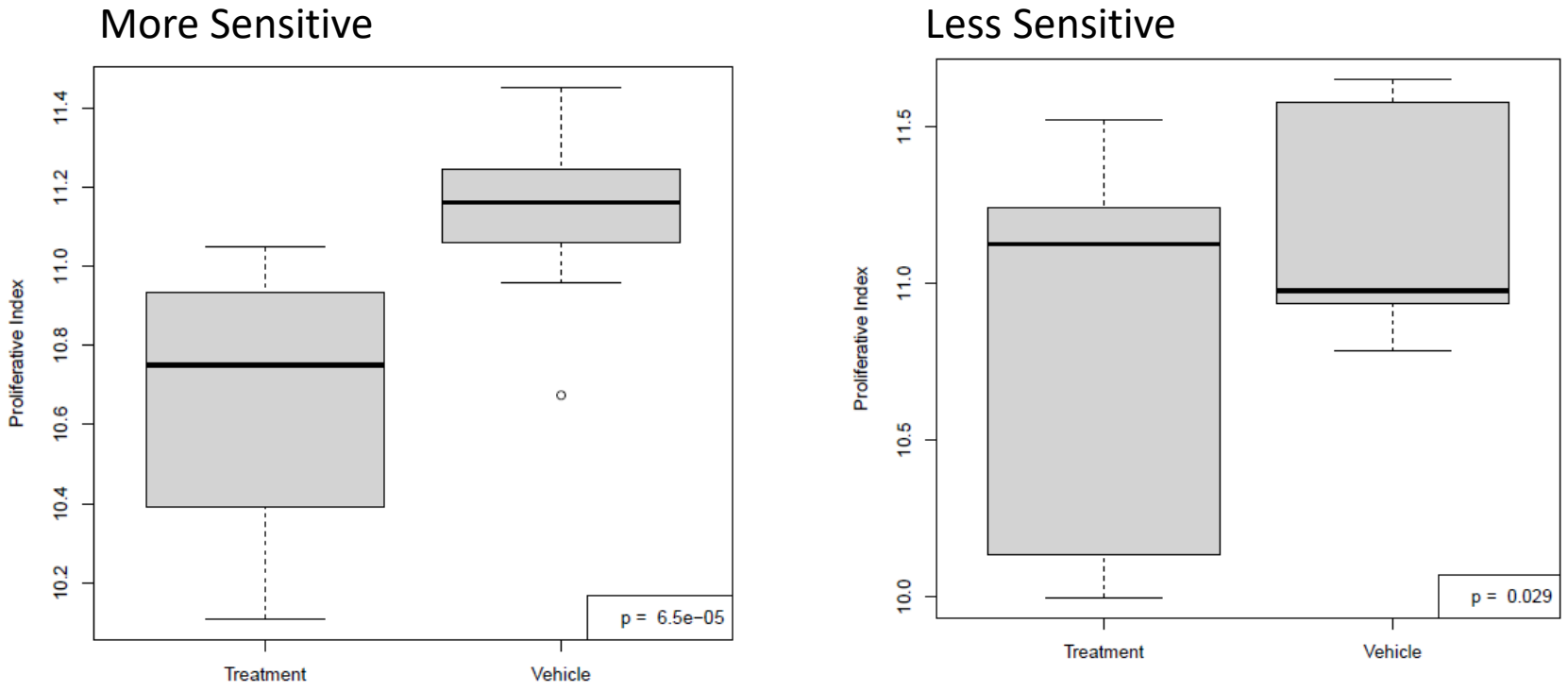

Supplementary Figure 10

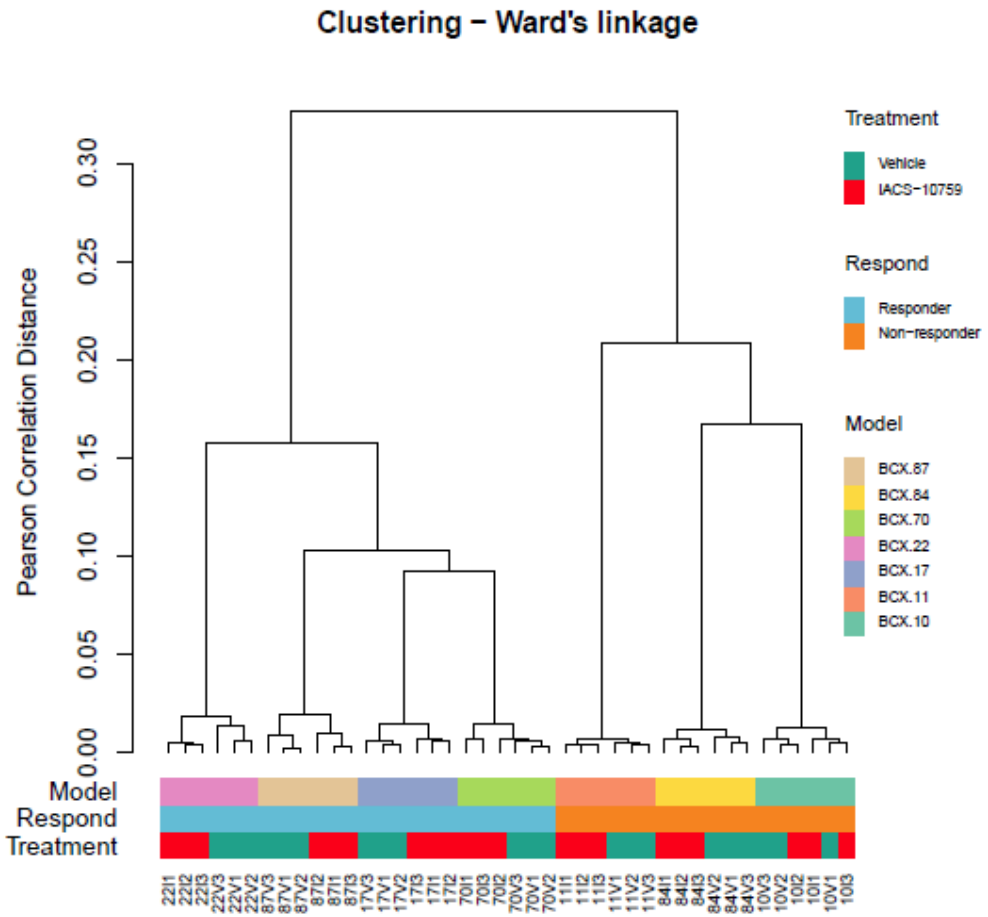

Supplementary Figure 11

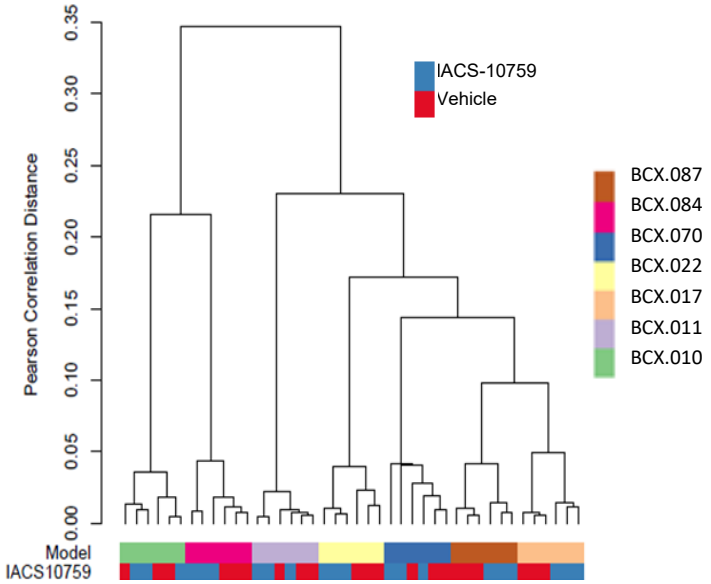

Supplementary Figure 12

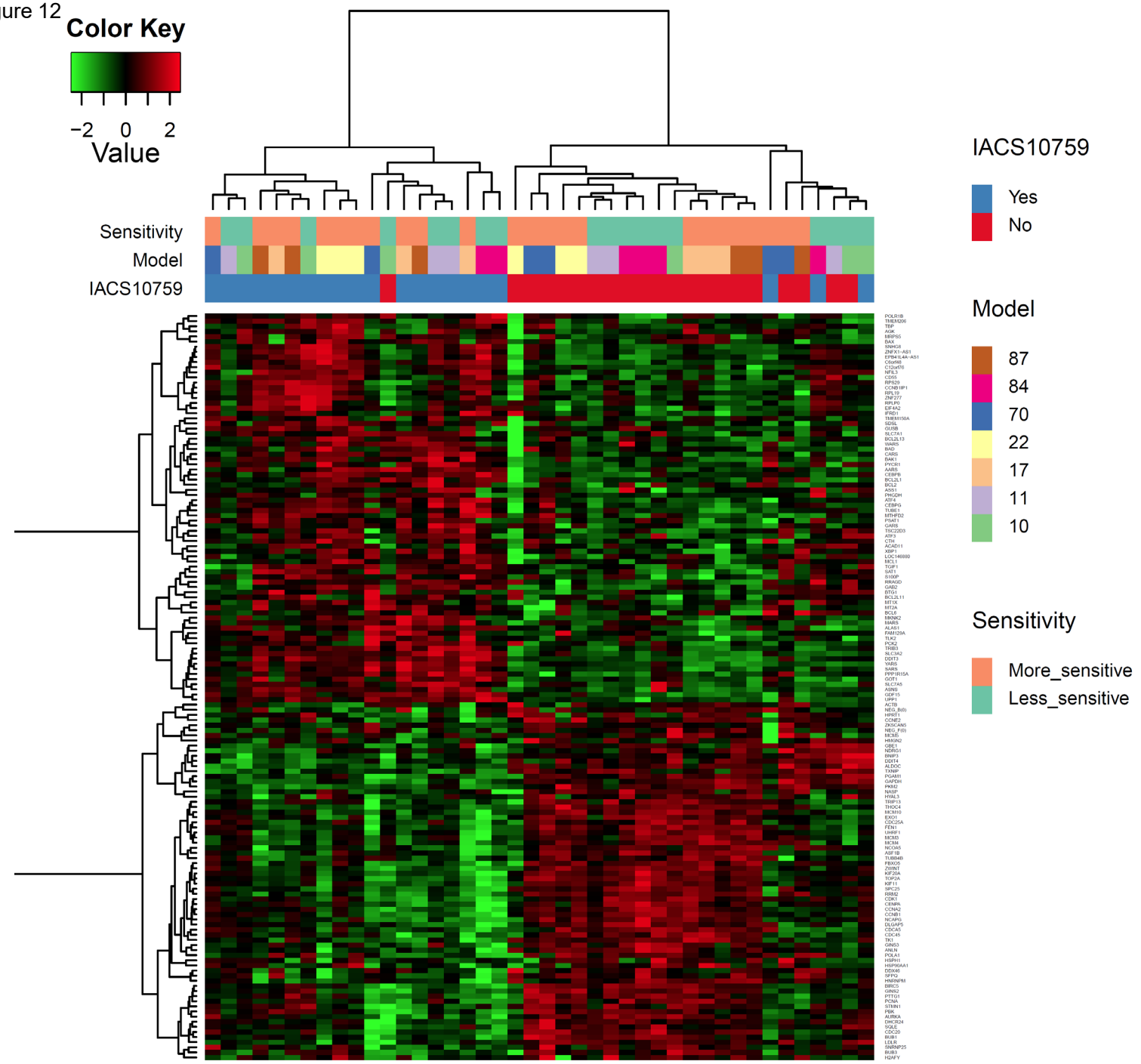

Supplementary Figure 13

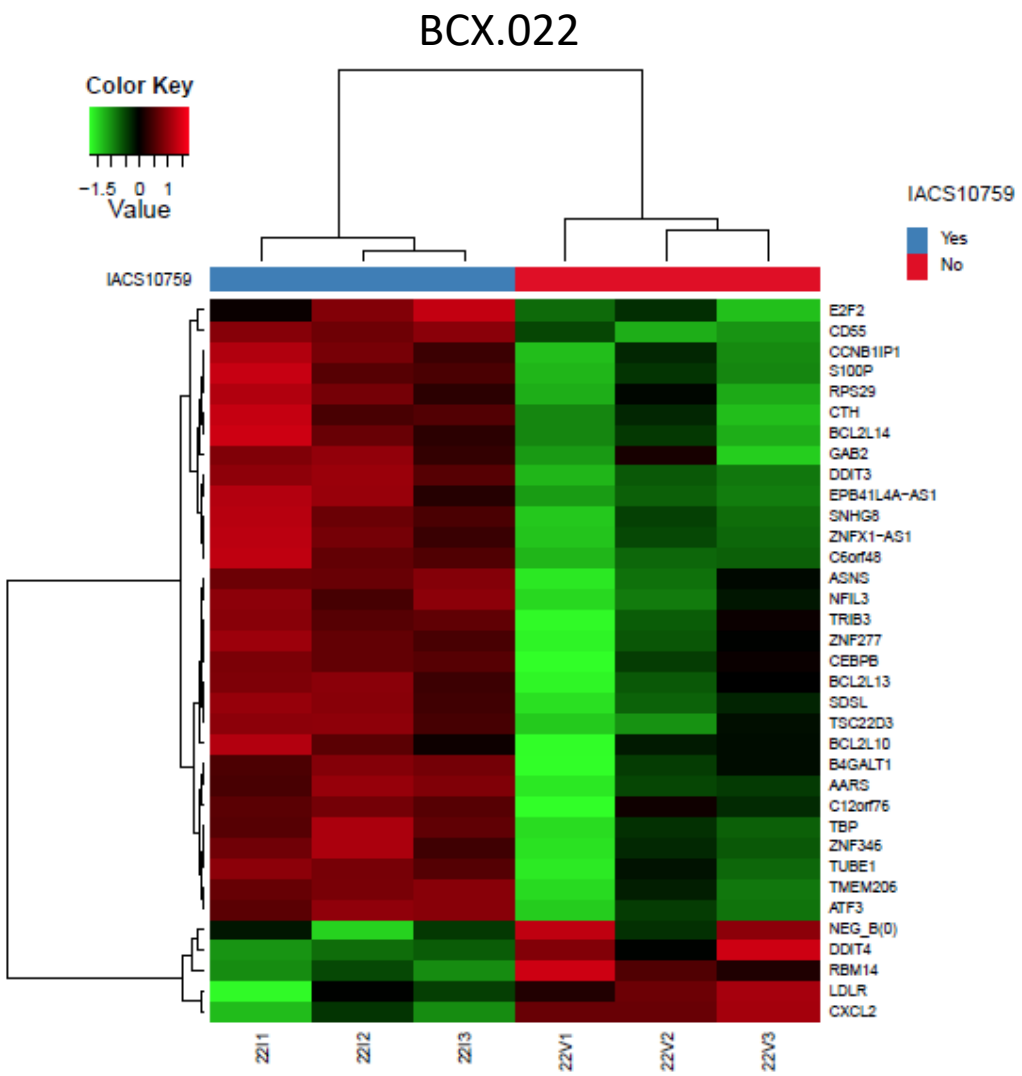

Supplementary Figure 14

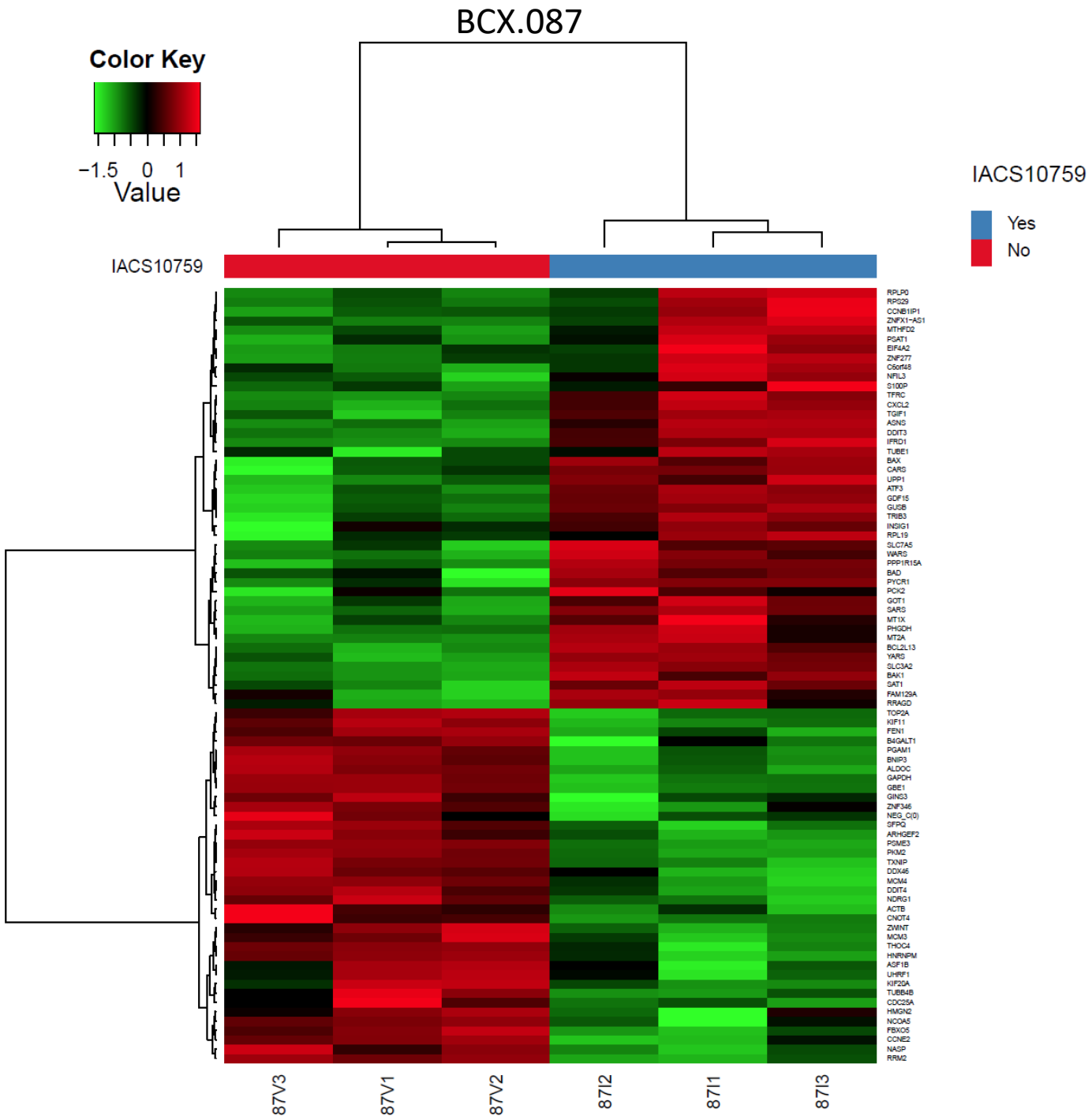

Supplementary Figure 15

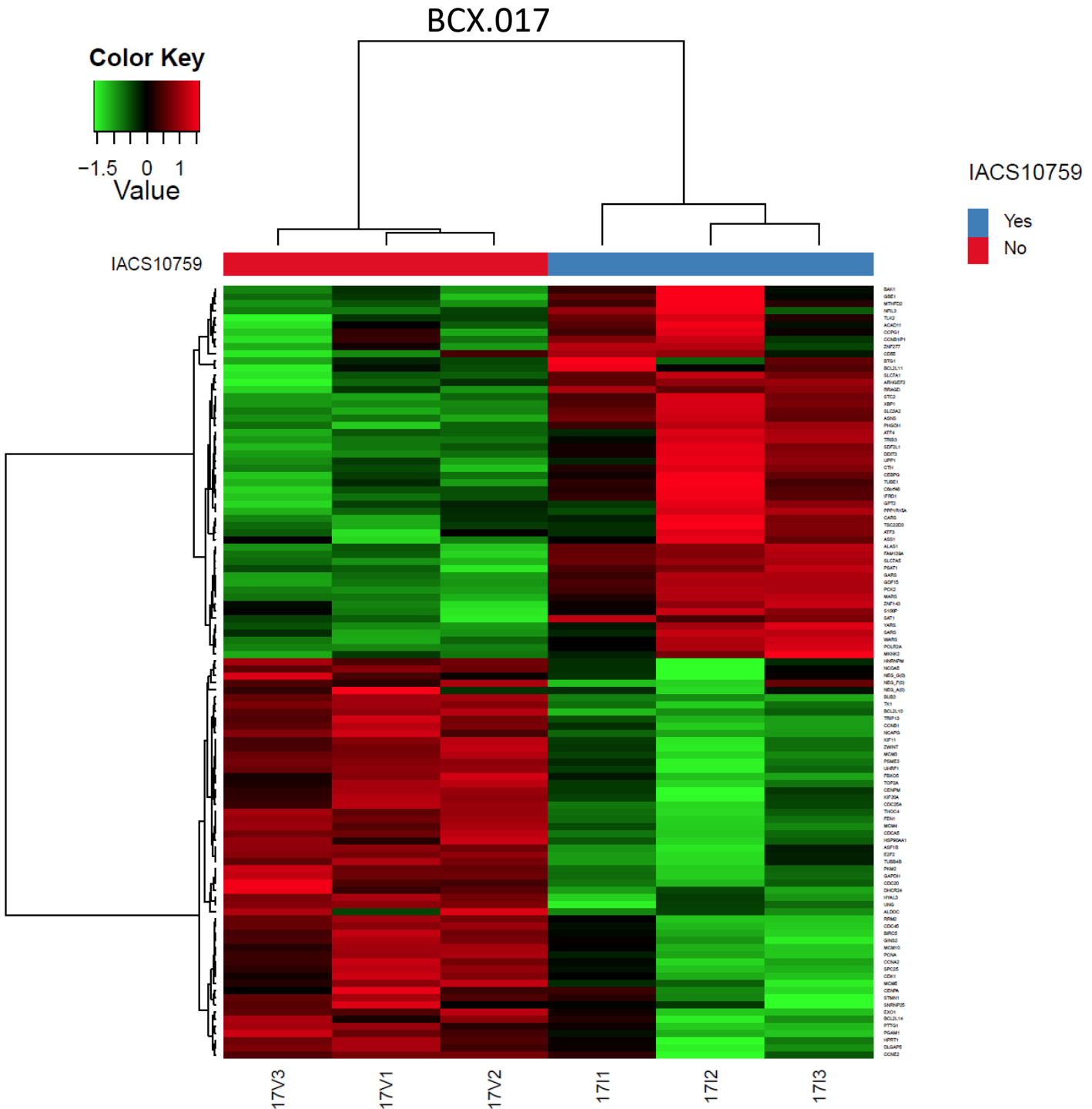

Supplementary Figure 16

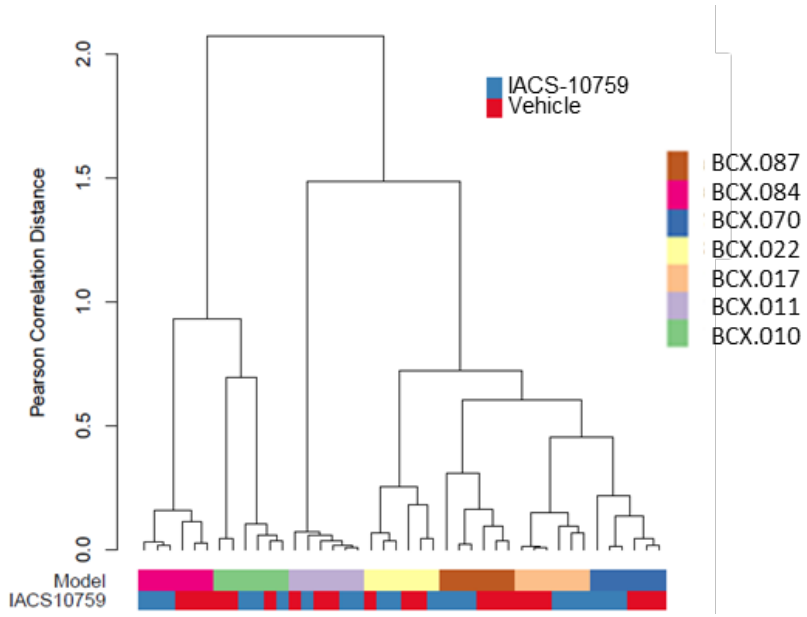

Supplementary Figure 17

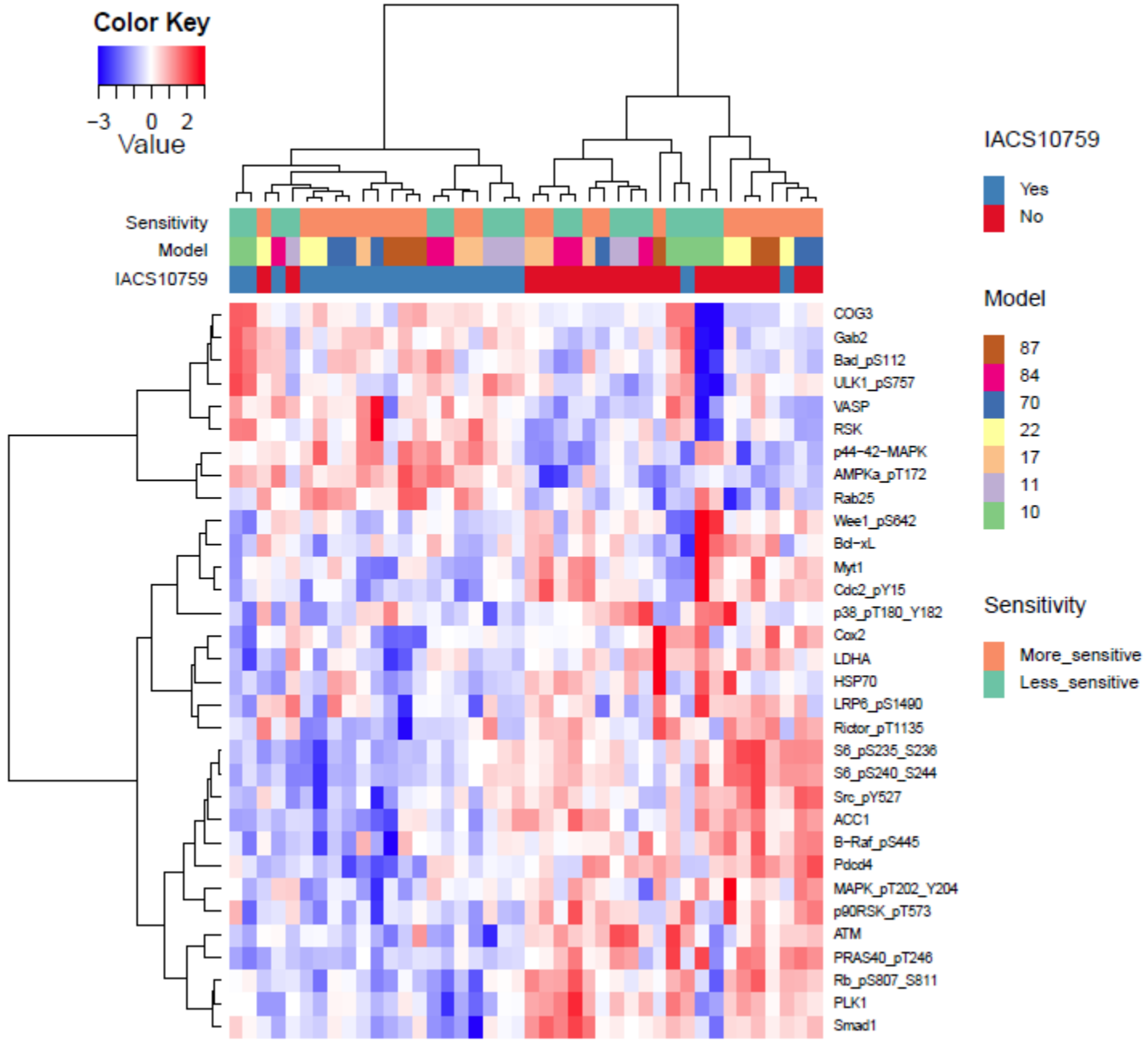

Supplementary Figure 18

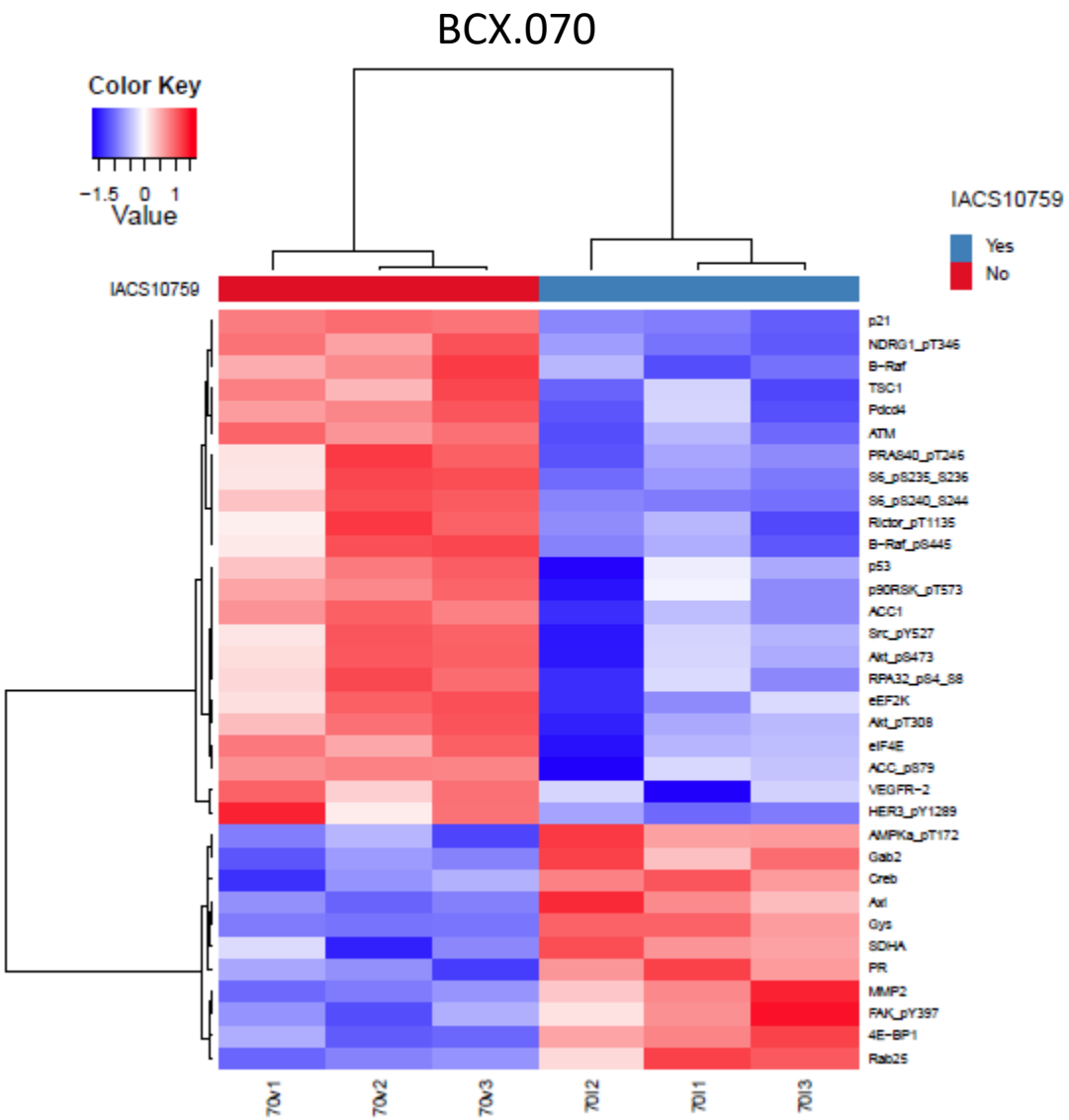

Supplementary Figure 19

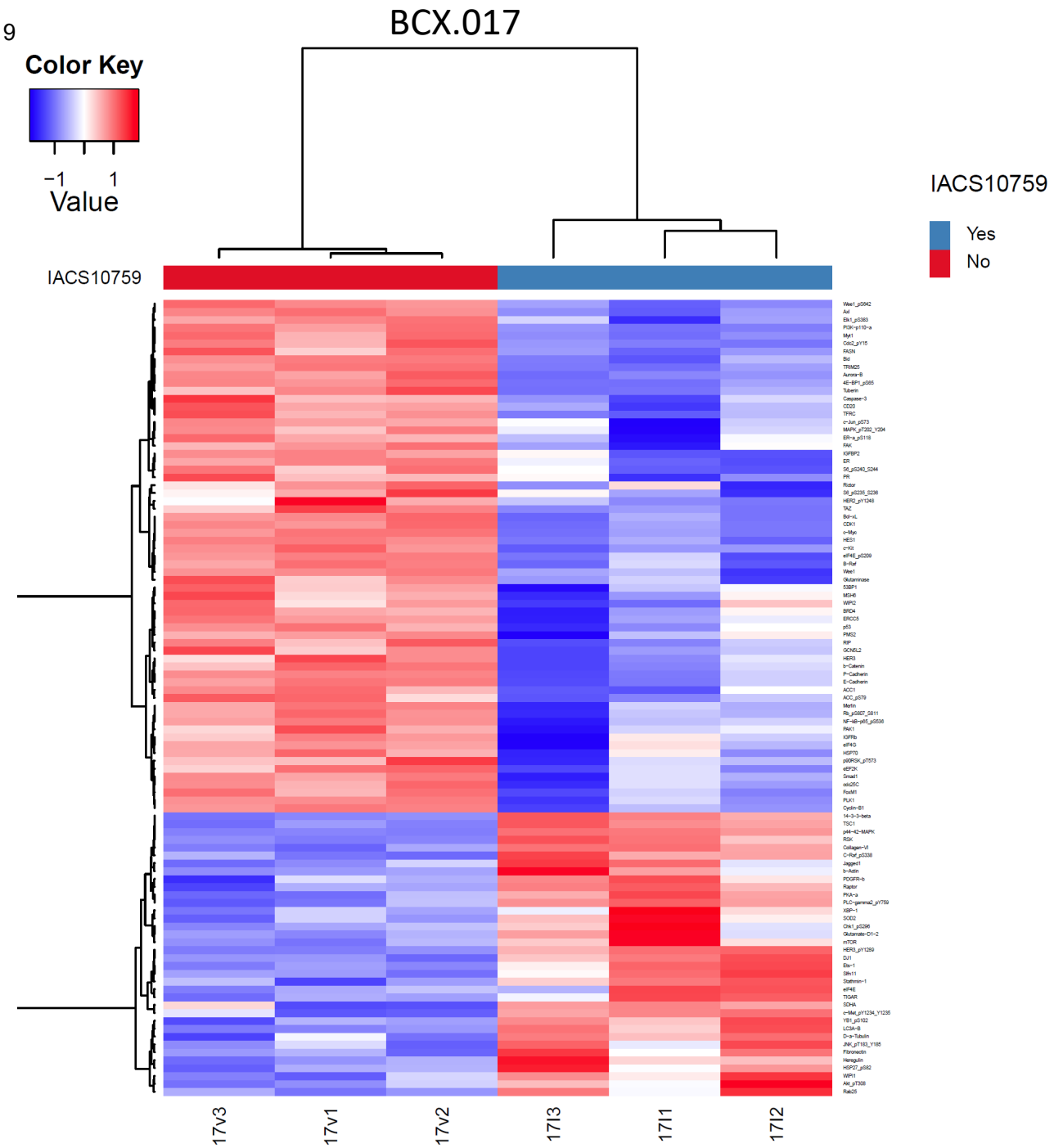

Supplementary Figure 20

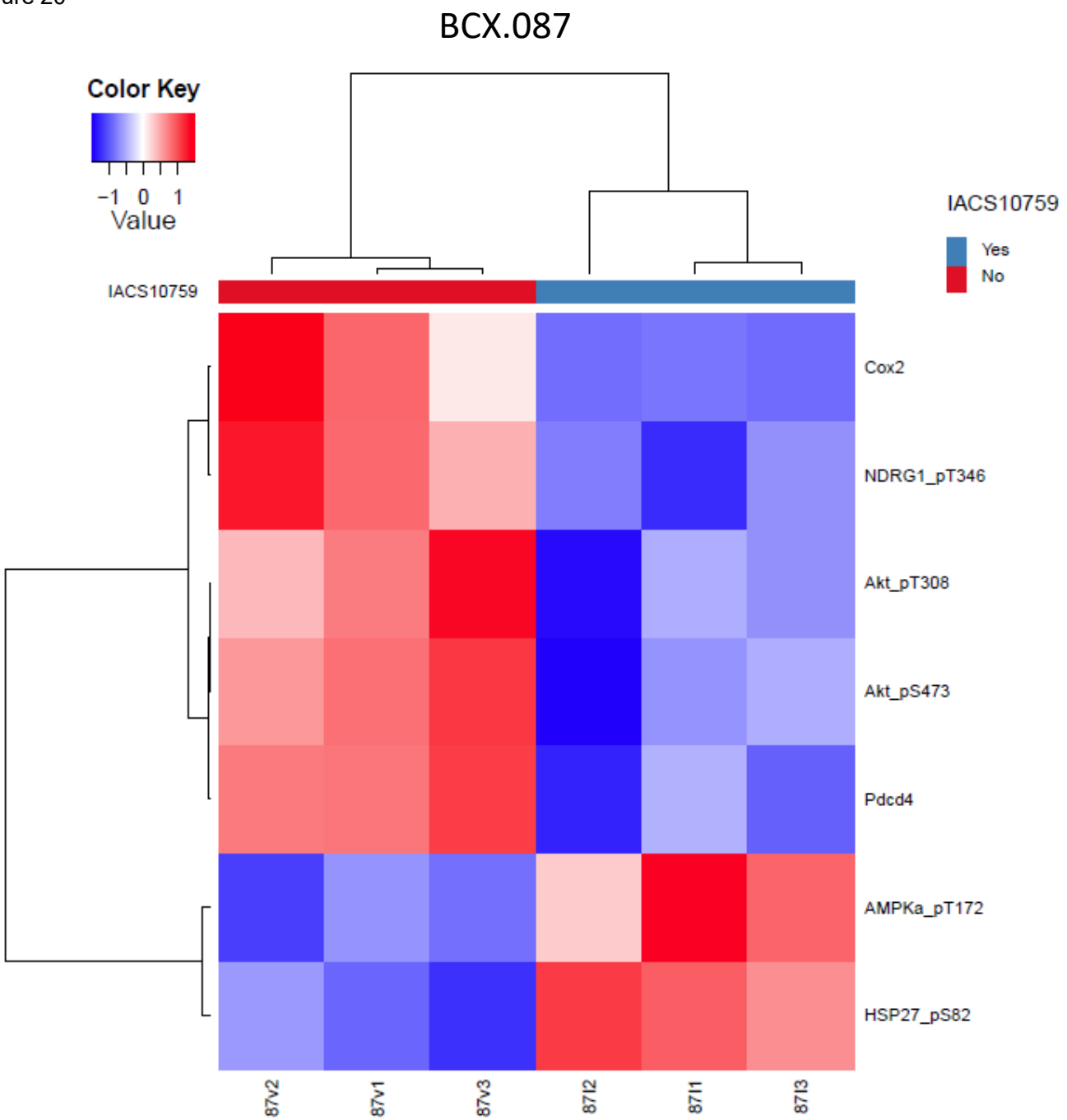

Supplementary Figure 21

A

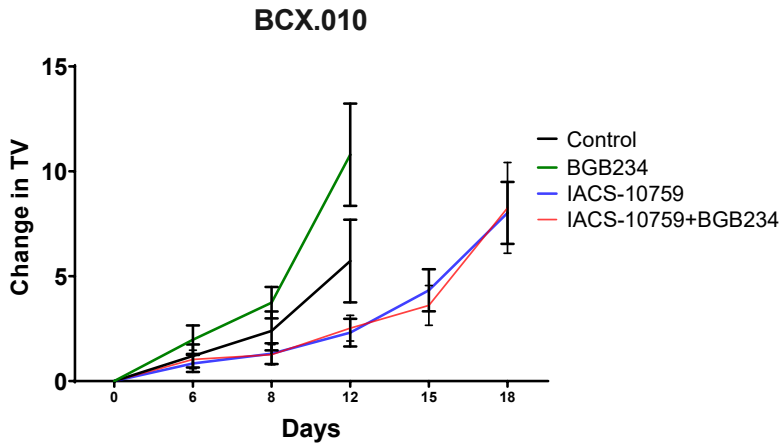

B

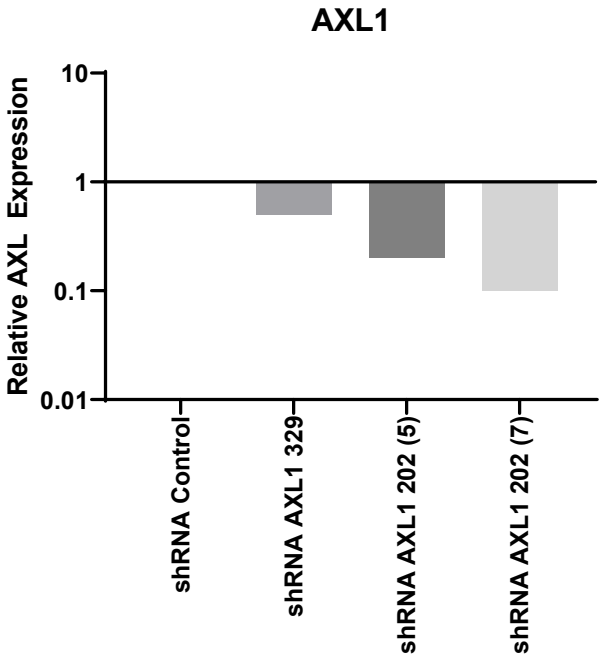

C

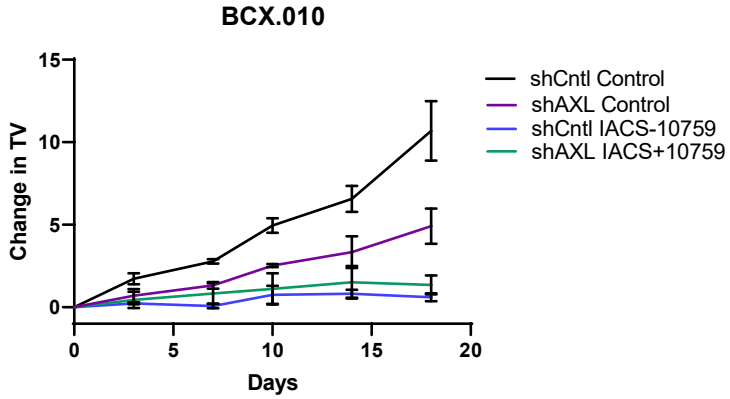

Supplementary Figure 22

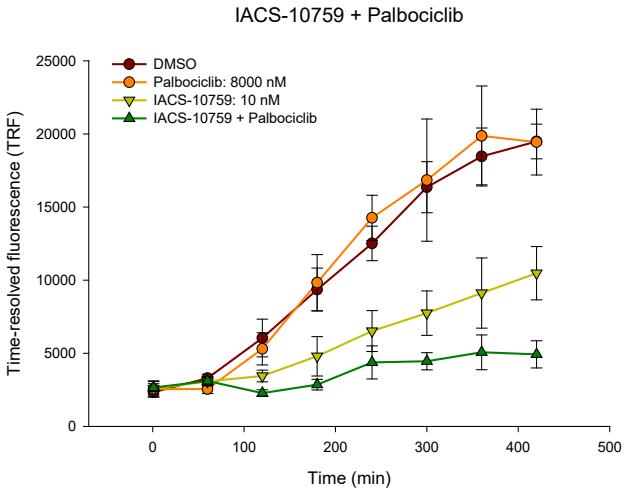

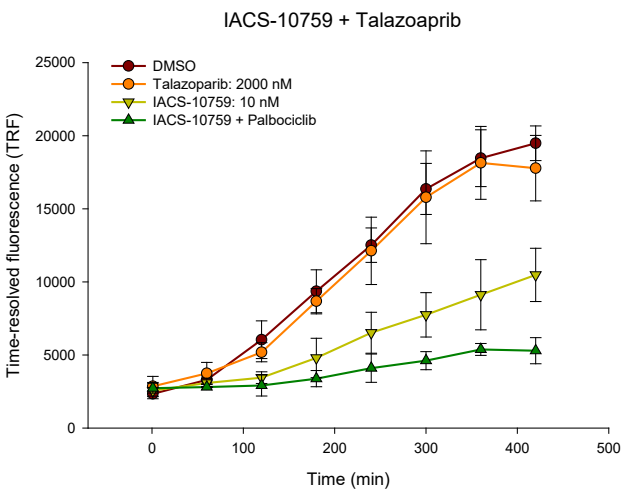

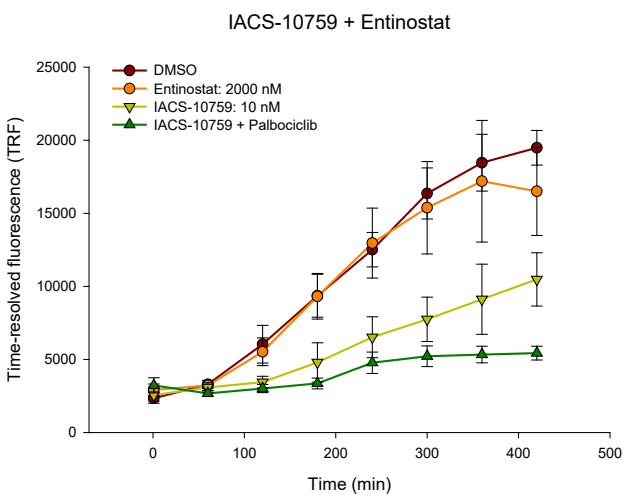

Supplementary Figure 23

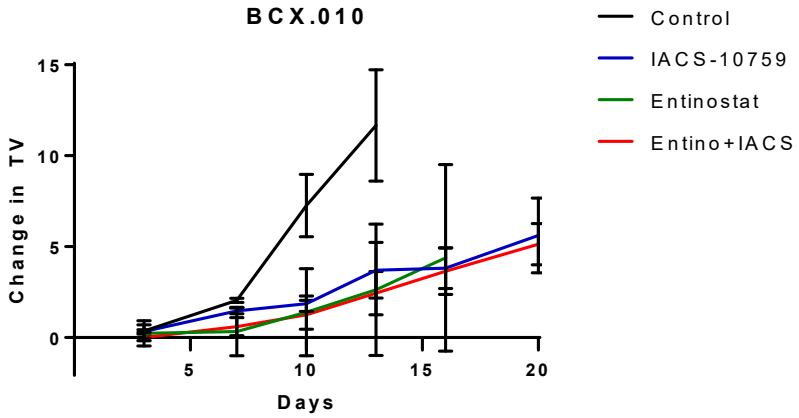

Supplementary Figure 1. We performed RNA sequencing on pre-treatment biopsies from 43 patients with operable TNBC who received sequential taxane-and anthracycline-based neoadjuvant chemotherapy. At greater than 5 year median follow-up, 12 patients had died. Heat map shows genes differentially expressed between patients who were alive or not at follow-up (false discovery rate of 0.05).

Supplementary Figure 2. Two TNBC PDXs were treated with BAY82-2243 (5 mg/kg, po, 5 days on 2 days off). Cohorts of at least 2-3 mice were used for this testing similar to the initial screen. Means +/- SEM are shown.

Supplementary Figure 3. Heatmap showing the expression of specific protein-encoding mitochondria genes at the RNA levels.

Supplementary Figure 4. ENO1 expression is lower in PDX that are more sensitive IACS-10759. (A) We accessed ENO1 RNA expression using RNAseq of early passage PDXs. (B) We performed IHC on a tissue microarray containing all the PDXs tested for IACS-10759 sensitivity. Each punch is a different area of the same tumor. ENO1 IHC was scored by a trained pathologist.

Supplementary Figure 5: Proliferative index at baseline for more versus less sensitive PDXs.
The p-value was calculated by fiting a linear mixed model.

Supplementary Figure 6. AXL expression as determine by western blot.

Supplementary Figure 7. On-treatment biomarkers of response to IACS-10759 in TNBC. We generated RNA expression data from 12-day treated samples. Global RNA expression cluster the sensitive models away from the less sensitive models, and in the case of the sensitive models, the treated samples clustered away from the respective untreated samples.

Supplementary Figure 8. IACS-10759 treatment downregulates several metabolic pathways. (A) Pathway analysis using RNA data from PDX treated for twelve days with IACS-10759 found that

hypoxia and lipid metabolism increased with IACS-01759 treatment and did so in a more pronounce fashion in sensitive models.

Supplementary Figure 9. Proliferative index in vehicle and IACS-10759 treatment groups for the more sensitive (A) and less sensitive models (B). The p-value was calculated by fitting a linear mixed model.

Supplementary Figure 10. Following removal of the gene included in the proliferative index from the overall RNAseq data, more sensitive PDXs still clustered separated from the less sensitive PDXs.

Supplementary Figure 11. On-treatment biomarkers of response to IACS-10759 in TNBC. We generated RNA expression data from 12-day treated samples using a Nanostring codeset designed based on expression changes related to modulation of oxidative phosphorylation in other diseases. We found that upon unsupervised clustering, the treated samples segregate away for the control samples regardless of model sensitivity.

Supplementary Figure 12. Genes differentially expressed between treated and untreated PDXs models as determine by a specific nanostring gene probe set.

Supplementary Figure 13. Genes differentially expressed between treated and untreated BCX.022, a sensitive model, as determine by a specific nanostring gene probe set.

Supplementary Figure 14. Genes differentially expressed between treated and untreated BCX.087, a sensitive model, as determine by a specific nanostring gene probe set.

Supplementary Figure 15. Genes differentially expressed between treated and untreated PDXs BCX.017, a sensitive model, as determine by a specific nanostring gene probe set.

Supplementary Figure 16. On-treatment biomarkers of response to IACS-10759 in TNBC. We generated proteomic data from 12-day treated samples using Reverse Phase Protein Arrays.

Proteomic data showed consistent profile changes with treatment and sensitive models clustered together.

Supplementary Figure 17. Proteins and phosphoprotein differentially expressed between treated and untreated PDXs models as determine by Reverse Phase Protein Arrays.

Supplementary Figure 18. Proteins and phosphoprotein differential expressed between treated and untreated BCX.070, a sensitive model, by Reverse Phase Protein Arrays.

Supplementary Figure 19. Proteins and phosphoprotein differentially expressed between treated and untreated BCX.017, a sensitive model, by Reverse Phase Protein Arrays.

Supplementary Figure 20. Proteins and phosphoprotein differentially expressed between treated and untreated BCX.087, a sensitive model, by Reverse Phase Protein Arrays.

Supplementary Figure 21. Specific Axl inhibition with BGB-324 and suppression do not have improve combination efficacy with IACS-10759. (A) We found no significant combination effects with BGB-324 (100 mg/kg/day, Chemietek) and IACS-10759 in BCX.010. (B and C) We suppressed expression Axl in BCX.010 using three different shRNA viral constructs and validated suppression using qRTPCR (B-C). We injected the control cell line and a validated stable shRNA cell lines back into mice and treated the mice with vehicle or IACS-10759 (n=4-5). While suppression of AXL and IACS-10759 alone had growth inhibitory effects, the combination did not improve efficacy. Means +/- SEM are shown.

Supplementary Figure 22. Effects of IACS-10759 combination on oxygen consumption *in vitro*. We used an Extracellular Oxygen Consumption Assay (Abcam) to determine effects of IACS-10759 and potential combination on oxygen consumption rate (OCR) for MDA-MB-468 over the course of seven hours. Besides IACS-10759, none of the other agents directly inhibited OCR, but the combinations of the agents led to a greater inhibition of OCR (X-axis).

Supplementary Figure 23. *In vivo* validation of the combination of IACS-10759 with entinostat. We tested entinostat (50 mg/kg daily) plus IACS-10759 in mice harboring BCX.010. Means +/- SEM are shown.